The Journal of Clinical Pharmacology
2018, 00(0) 1–14

DOI: 10.1002/jcph.1133

Development of a Physiologically Based Pharmacokinetic Model of Ethionamide in the Pediatric Population by Integrating Flavin-Containing Monooxygenase 3 Maturational Changes Over Time

Phuong Thi Thu Nguyen, MD, MS[1,2], Md Masud Parvez, PhD[1,3], Min Jung Kim, PhD[1], Jung Ho Lee, MD, PhD[1], Sangzin Ahn, MD, PhD[1], Jong-Lyul Ghim, MD, PhD[1,4], and Jae-Gook Shin, MD, PhD[1,4]

Abstract

Currently, ethionamide is the most frequently prescribed second-line antituberculosis drug in children. After extensive metabolism by flavin-containing monooxygenase (FMO) isoform 3 in the liver, the drug may exert cytotoxic effects. The comparison of children in different age groups revealed a significant age-related increase in ethionamide elimination in vivo. However, to date, the exact mechanism underlying this dynamic increase in ethionamide elimination has not been elucidated. We hypothesized that the age-dependent changes in ethionamide elimination were predominantly a result of the progressive increases in the expression and metabolic capacity of FMO3 during childhood. To test this hypothesis, a full physiologically based pharmacokinetic (PBPK) model of ethionamide was established and validated in adults through incorporation of comprehensive metabolism and transporter profiles, then expanded to the pediatric population through integration of FMO3 maturational changes over time. Thus, a good prediction PBPK model was validated successfully both in adults and children and applied to demonstrate the critical contribution of FMO3 in the mechanistic elimination pathway of ethionamide. In addition, a significant correlation between clearance and age was observed in children by accounting for ethionamide maturation, which could offer a mechanistic understanding of the age-associated changes in ethionamide elimination. In conclusion, this study underlines the benefits of in vitro-in vivo extrapolation and a quantitative PBPK approach for the investigation of transporter-enzyme interplay in ethionamide disposition and the demonstration of FMO3 ontogeny in children.

Keywords

ethionamide, FMO3, PBPK, pediatric, ontogeny

Drug-resistant tuberculosis is a continuing threat to the health of the world's population. In 2016, the World Health Organization reported there were 600,000 new cases of resistance to rifampicin, of which 490,000 were multidrug-resistant tuberculosis.[1] As an oral second-line drug, ethionamide is strongly recommended by the World Health Organization for the treatment of multidrug-resistant tuberculosis in both adults and children.[2] Owing to the global emergence and spread of multidrug-resistant tuberculosis, ethionamide has become increasingly used as a replacement therapy for cases of isoniazid- and rifampicin-resistant tuberculosis.[3] A systematic review of children treated for multidrug-resistant tuberculosis reported combination therapy success of 81.67%; ethionamide was a part of the drug regimen in all the studies included.[4] Ethionamide is a prodrug predominantly metabolized by flavin-containing monooxygenases (FMOs), including FMO2 and FMO3.[5] It has minimal urinary excretion (<1% of the administered parent drug dose)[5–8] to form the active metabolite ethionamide sulfoxide, which determines the therapeutic effect and the toxicity of ethionamide. FMO2 is expressed predominantly in human lungs as a truncated protein, whereas FMO3 has been proven to be the major form of FMO in the adult human liver.[5,9]

[1]Department of Pharmacology and PharmacoGenomics Research Center, Inje University College of Medicine, Busan, Republic of Korea
[2]Faculty of Pharmacy, Hai Phong University of Medicine and Pharmacy, Haiphong, Vietnam
[3]Leslie Dan Faculty of Pharmacy, University of Toronto, Toronto, Canada
[4]Department of Clinical Pharmacology, Inje University Busan Paik Hospital, Busan, Republic of Korea

Submitted for publication 7 February 2018; accepted 14 March 2018.

Corresponding Author:
Jae-Gook Shin, MD, PhD, Department of Pharmacology and PharmacoGenomics Research Center, Inje University College of Medicine, Busan, Republic of Korea
E-mail: phshinjg@inje.ac.kr

In adults, the absorption of ethionamide takes place wholly within the gastrointestinal tract, and food has a minor effect on this process. After absorption, ethionamide is distributed widely into body fluids and various tissues.[10] In a pediatric-specific pharmacokinetic (PK) study, significantly lower ethionamide exposure (maximum observed plasma concentration [C_{max}] and area under the plasma drug concentration-time curve [AUC]) was reported in tuberculosis-infected children younger than 2 years when compared with older age groups administered the same oral dose (mg/kg).[11] This finding may indicate a need for a higher dose in the young age group. In addition, a significant correlation between age and ethionamide elimination was reported after 1 month of ethionamide therapy,[11,12] which indicated that age may be an additional covariate, along with body weight, for determination of ethionamide dose adjustment in pediatric indications. However, the mechanistic cause of dynamic changes related to age with ethionamide exposure is not well understood.[11] Coupled with clinical findings, developmental changes in the metabolic function of FMO3 during childhood were indicated in in vivo phenotype tests, as well as in vitro liver microsomal quantification.[13–16] An additional mechanistic understanding of the fundamental metabolic pathway and the effect of the maturational process of FMO3 can assist in ethionamide dosing decisions in children.

For an accurate prediction, an understanding of the contribution of the interplay of drug transporters and enzymes to overall absorption, distribution, metabolism, and excretion based on mechanistic in vitro-in vivo extrapolation techniques is required.[17] Consequently, an additional in vitro metabolism experiment using pooled human liver and lung microsomes was conducted in this study for allometric scaling to predict in vivo intrinsic clearance.[18–20] Additionally, our comprehensive in vitro transporter study of 22 antituberculosis drugs in cells overexpressing solute carrier and adenosine triphosphate–binding cassette transporters indicates that ethionamide is a highly permeable drug with substrate affinity to multiple efflux transporters, including multidrug resistance protein 1/P-glycoprotein (MDR1/P-gp), multidrug resistance-associated protein 1 (MRP1), and multidrug resistance-associated protein 2 (MRP2) (unpublished data). Subsequently, the transport and metabolism kinetic data were used to simulate the absorption, distribution, metabolism, and excretion of ethionamide using physiologically based pharmacokinetic (PBPK) modeling and simulation.

We hypothesized that the causal mechanism for change in ethionamide exposure with increasing age in children was mostly FMO3 maturational changes over time. To test the hypothesis, we conducted 1) an in vitro metabolism experiment using pooled human liver and lung microsomes and 2) established a PBPK model for ethionamide by incorporating in vitro metabolism and transporter profiles, verified it in adults, then expanded the model for application in the pediatric population, over the entire pediatric age range, through the integration of FMO3 maturational changes with time. The final, well-established PBPK model was subsequently applied to evaluate the effect of FMO3 ontogeny on ethionamide elimination.

Materials and Methods

Ethionamide was purchased from Sigma-Aldrich (Sigma-Aldrich Korea Ltd, Seoul, Republic of Korea). Ethionamide sulfoxide was supplied by Toronto Research Chemicals (Ontario, Canada). Other reagents used in the present study were obtained from commercial companies. Pooled human liver microsomes (13 female donors and 17 male donors; lot 28831) were provided by BD Biosciences (San Jose, California). Pooled human lung microsomes (2 female donors and 2 male donors; lot 1510341) were purchased from Xenotech (Kansas City, Kansas).

Metabolism Studies Using Pooled Human Liver Microsomes and Pooled Human Lung Microsomes

The final volume of the incubation mixture was 100 μL. Pooled human liver microsomes and pooled human lung microsomes, both at a final protein concentration of 0.1 mg/h/L, were incubated at 37°C with 100 mM phosphate buffer (pH 7.4), nicotinamide adenine dinucleotide phosphate-oxidase (1 mM), and ethionamide for 30 minutes. Ethionamide concentrations 1, 5, 10, 50, 100, 250, and 500 μM were used for reaction. The reactions were stopped by the addition of 100 μL acetonitrile on ice, followed by centrifugation at 16,000 × g for 5 minutes. Finally, the supernatants were analyzed by liquid chromatography tandem mass spectrometry (LC-MS/MS).

Transport Study Using Stably Transfected Cell Lines. Transport experiments were conducted in accordance with our previously published method.[21] Briefly, porcine kidney-derived cell line (LLC-PK1)-P-gp, Madin-Darby canine kidney II (MDCKII)-MRP1, and MDCKII-MRP2 were seeded at a density of 2.5×10^5 cells per well in 24-well plates and cultured for 5 days to reach sufficient confluency. The kinetic parameters K_m and V_{max} were calculated using a concentration-dependent bidirectional transport assay for LLC-PK1-P-gp, MDCKII-MRP1, and MDCKII-MRP2, as summarized in Table 2.

LC-MS/MS Analysis. The LC-MS/MS method for the quantitation of ethionamide and ethionamide sulfoxide

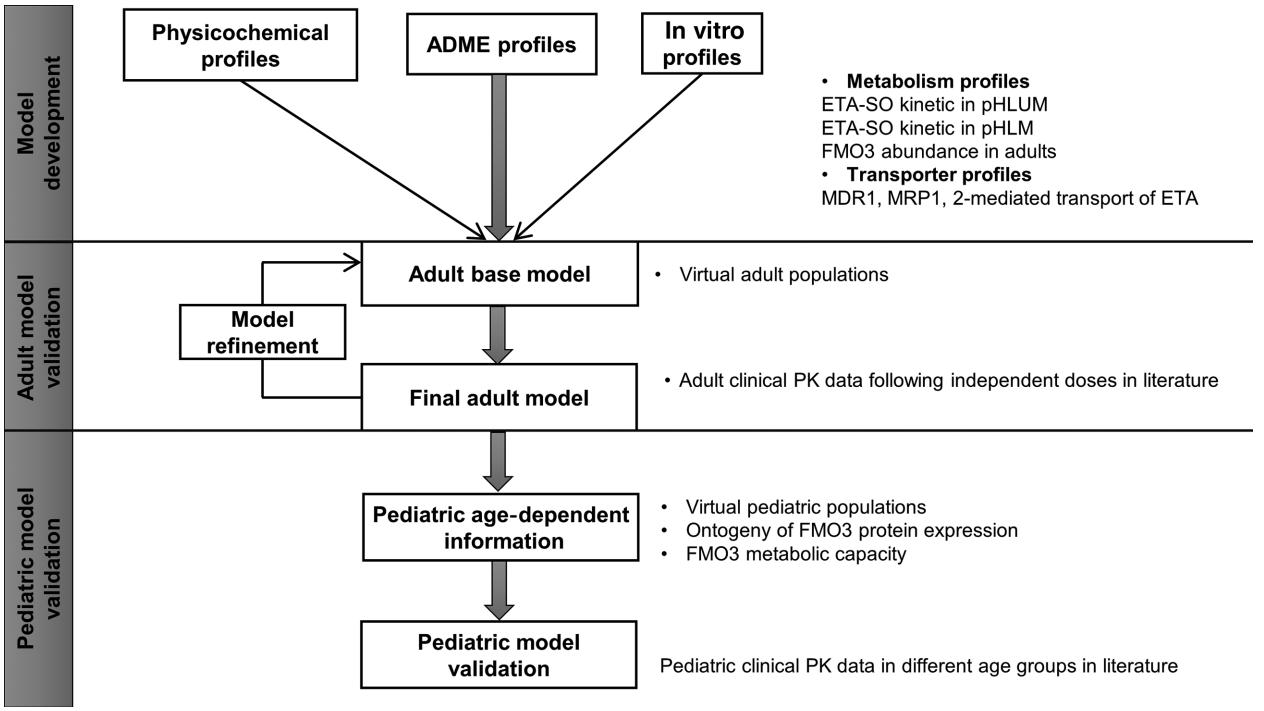

Figure 1. A proposed framework for the application of PBPK modeling. An ethionamide PBPK model in the pediatric population was constructed by integration of multiple levels of in silico, in vitro, and in vivo data.

was performed in accordance with a previous report.[22] Briefly, high-performance liquid chromatography was performed on an Agilent 6410 Triple Quadrupole LC/MS system (Agilent Technologies, Santa Clara, California). The separation was performed on Xbridge C18 column (150 × 2.1 mm, 3 μm; Waters, Milford, Massachusetts). The mobile phase comprised (A) 100% distilled water containing 0.1% formic acid and (B) 100% acetonitrile containing 0.1% formic acid. The mobile phase was eluted using an Agilent 1200 series pump (Agilent Technologies) at a flow rate of 0.25 mL/min, and 0.1 μL was injected. The mass spectra of ethionamide and ethionamide sulfoxide were recorded by electrospray ionization in positive ion mode. The turbo ion spray interface was set at 5500 V and 600°C. Multiple reaction monitoring modes using specific precursor-to-product ion transitions were performed for the quantification of ethionamide and its metabolite. Ethionamide was detected at ion transitions of m/z 167.1 → 107.0, whereas ethionamide sulfoxide was detected at the transitions of m/z 183.1 → 107.0. Rifabutin and linezolid were used as internal standards for the detection of ethionamide and ethionamide sulfoxide. The peak areas of all compounds were automatically incorporated using MassHunter quantitative analysis (version B.1.5.2; Agilent Technologies).

Modeling Strategy

In general, the comprehensive development process of a PBPK model of ethionamide in the pediatric population followed the guidelines of the US Food and Drug Administration, as outlined in Figure 1.[23,24] The modeling strategy was implemented as follows: 1) Ethionamide metabolism was determined by quantification of the velocity of ethionamide sulfoxide formation in the pooled human liver and lung microsomes. 2) The ethionamide PBPK model in the adult population was developed by incorporating in vitro, in silico, and in vivo data. 3) The developed model in adults was validated through comparison with the available clinical data. 4) The verified adult model was then expanded for the prediction of ethionamide PK in children of 3 age categories (0 months-2 years; 2-6 years, 6-12 years). In the pediatric PBPK model, we used the same physicochemical properties of ethionamide and replaced age-dependent protein abundance, metabolic kinetics of FMO3, and age-associated anatomic and physiological changes using a virtual pediatric population in a Simcyp simulator (version 15 release 1, Certara, Sheffield, UK) (Table 2). 5) Pediatric PBPK models were used for further evaluation against observed clinical data in children in the 3 corresponding age groups.

Development of Ethionamide PBPK Model in Adult and Pediatric Populations

There are two default white adult population databases in the Simcyp simulator population library. The first database is the "Healthy North European Caucasian Volunteers," which was constructed based on demographic information for 19- to 65-year-olds; the

second is the "General North European Caucasian" database of 18- to 95-year-olds. Virtual populations were matched to the volunteers of the corresponding observed study for demographic information (age, height, weight, sex, and ethnicity). Thus, the first database was chosen for the simulation of a 500-mg single oral dose of ethionamide PK in adults aged 29-43 years and a female proportion of 0.075.[25] The second database was used to predict the ethionamide exposure following a single dose of 250 mg in adults aged 18-53 years and a female proportion of 0.5.[10]

FMO3 abundance in the liver was determined from a literature analysis of 3 separate studies. Only data from adult whites (older than 16 years) were selected. Finally, a mean value of 59.3 pmol/mg human liver microsomes with a 38% coefficient of variation (CV), calculated from 3 studies,[15,26,27] as listed in Table 1, was incorporated into the virtual adult population.

The default virtual pediatric populations in the Simcyp population-based simulator, with extensive libraries on demographics and the developmental physiology associated with FMO3 maturation, were used to create the virtual duplicates of clinical studies for simulating an ethionamide model in children. Microsomal FMO3 protein content from 240 liver samples representative of children aged 8 weeks-18 years[13] and 199 liver samples representative of children aged 0-18 years[15] previously reported were used to estimate the weighted mean value (CV%) of FMO3 for the following 3 age groups: (1) 0-2 years: 7.9 pmol/mg (75.4%); (2) 2-6 years: 16.9 pmol/mg (58.2%); (3) 6-12 years: 22.1 pmol/mg (49.6%). The calculation for the FMO3 abundance in children is shown in Table 1.

Together with the mean value, FMO3 ontogeny was fitted using a nonlinear regression formulation (equation 2) in R software (R Foundation, Vienna, Austria),[28] as reported previously[29]:

$$F = \left(\frac{Adult_{max} - F_{birth}}{Age_{50}^{n} + Age^{n}}\right) \times Age^{n} + F_{birth} \quad (1)$$

where $Adult_{max}$ is the maximum average relative protein abundance, Age is the age in years of the subject at the time of sample collection, Age_{50} is the age in years at which the half-maximum adult protein abundance is obtained, F is the fractional protein abundance at a given age, F_{birth} is the fractional protein abundance (of adult) at birth, and n is the exponential factor. The values of F_{birth}, $Adult_{max}$, Age_{50}, and n were determined as 0.86, 25.95, 0.80, and 0.49, respectively, and were integrated into the virtual pediatric population.

Although the functional metabolic capacity of FMO3 was significantly decreased (–40%) in children in the 0-2 years group, in the older age groups, the catalytic efficiency was similar to adults.[16] Therefore, the intrinsic clearance (CL_{int}) of FMO3 in the 0- to 2-year-old group was defined as 6.43 (μL/min/mg microsomal protein).

The physicochemical properties and in vitro data used in PBPK model development, along with the source, are outlined in Table 2. The advanced dissolution absorption metabolism model within the Simcyp population-based absorption, distribution, metabolism, and excretion simulator was selected for absorption.[30] A full PBPK model following the Rodgers and Rowland method[31] (Method 2), which accounted for the rapid equilibrium between blood and tissues (except gut, liver, and lungs), was adopted to model ethionamide distribution into all organs. In the case of hepatic and lung disposition, the permeability-limited model was considered, wherein the intrinsic clearance of canalicular active efflux transporters, including P-gp, MRP1, and MRP2, were incorporated.

The extrapolation of in vivo lung clearance from in vitro intrinsic clearance in pooled human lung microsomes was represented using Michaelis-Menten kinetics, as shown by the following equation:

$$CLu_{lung,int} = \left(\frac{V_{max}}{K_m \times fu_{mic}}\right) \times MPPGLU \times Lung\ weight \quad (2)$$

MPPGLU is milligrams of microsomal protein per gram of lung, as reported by Prough RA,[32] with the value of 2.27 mg/g, and fu_{mic} is the fraction of unbound drug in the in vitro microsomal incubation. The total right and left human lung weight were observed[33] (mean value of 840 g in adults). The data for lung weight in children were obtained from a previous study,[34] which reported a mean value of 156.4 g for the 0- to 2-year-old group, 316.7 g for the 2- to 6-year-old group, and 438.3 g for the 6- to 12-year-old group. Thus, the in vivo lung clearance (L/h) in children of the 3 age groups and adults was predicted as 2.1, 4.2, 5.8, and 11.2, respectively.

The sensitive analysis technique is required in addition to PBPK modeling and simulation to assess the influence of different factors on the drug response and explore the interaction between individual parameters.[35] Therefore, to provide insight into the effect of metabolizing enzymes and transporters on ethionamide disposition, sensitivity analyses focusing on FMO2 and FMO3 intrinsic activity were performed to explore their potential effects on ethionamide clearance and absorption rate (C_{max}) by expanding the ethionamide PBPK model after a single dose of 500-mg ethionamide in adults. The maximum CL_{int} value of FMO2, FMO3, and transporter kinetics were modified

Table 1. Input Parameter for FMO3 Abundance in Adults and Children

		FMO3 Content (pmol/mg)	Reference
FMO3 abundance in adult liver[a]		69.8 (53)	25
		80.0 (50)	26
		28.0 (39)	15
Mean (CV)		59.3 (38)	
FMO3 abundance in child liver[b]	0-3 weeks	1.1	13
	3 weeks-10 months	4.7	13
	10 months-11 years	12.7	13
	11-18 years	26.9	13
	0-1 years	14.4	15
	1-6 years	20.0	15
	6-12 years od	24.6	15
Mean (CV)[a]	0-2 years	7.9 (75.4)	
	2-6 years	16.9 (58.2)	
	6-12 years	22.1 (49.6)	

[a]Data presented as mean (coefficient of variation).
[b]Data presented as mean.

Table 2. Ethionamide Input Parameters in PBPK Models

Parameter (Unit)	Value	Reference	
1. Physicochemical Properties and Blood Binding			
Molecular weight (g/mol)	166.25	Internal data	
f_u	0.7	Internal data	
Blood-to-plasma ratio (B:P)	0.55	Simcyp predicted	
logPo:w	1.74	Internal data	
Compound type	Monoprotic acid	54	
pK_a	4.49	55	
Main plasma protein binding	HSA	56	
2. Absorption Model	Advanced Dissolution, Absorption, and Metabolism Model		
fu_{gut}	0.98	Simcyp predicted	
Q_{Gut} (L/h)	14.19	Simcyp predicted	
Caco-2 (A-B) (10^{-6} cm/s)	57.3	55	
$P_{eff,man}$ (10^{-6} cm/s)	6.33	Simcyp predicted	
3. Distribution Model	Full PBPK Model		
V_{ss} (L/kg)	0.42	Simcyp predicted	
4. Elimination Model	Enzyme kinetics		
ETA-SO formation in liver	K_m (μM) $\pm$ SD	147.3 $\pm$ 27.32	In-house data (Figure 2)
	V_{max} (pmol/min/mg protein) $\pm$ SD	1987.9 $\pm$ 128.29	
	fu_{mic}	0.9	
CL_R (l/h)	0.23		Calculated from[7]
CL_{lung} (l/h)	11.24		Described in method
Additional liver clearance (μL/min/mg protein)	4.87		Representing about 26.5% of ETA clearance in liver[5]
Permeability limited liver model (Active efflux transporter kinetics)			
LLCPK1 transfected cells MDR1			In-house unpublished data
	K_m (μM)	238	
	V_{max} (pmol/min/10^6 cells)	1120	
	RAF/REF	1.5[57]	
MDCKII transfected cells MRP2	K_m (μM)	166	
	V_{max} (pmol/min/10^6 cells)	1856	
	RAF/REF	1	
MDCKII transfected cells MRP1	K_m (μM)	71	
	V_{max} (pmol/min/10^6 cells)	684	
	RAF/REF	1	

logPo:w, octanol, water partition coefficient; f_u, unbound fraction; pKa, ionization coefficient; HSA, human serum albumin; PSA, polar surface area; V_{ss}, volume of distribution at steady state; CL_R, renal clearance; CL_{lung}, lung clearance; ETA-SO, ethionamide sulfoxide; MDCKII, Madin-Darby canine kidney II; LLCPK1, porcine kidney-derived cell line; P_{eff}, effective permeability.

from 100% to 0 of the control value (set at 100%), as listed in Table 2.

The correlation between ethionamide systemic clearance and age was evaluated by the performance of a 10-trial simulation in virtual pediatric subjects. The median prediction trends of systemic clearance values expressed in 2 scenarios (with and without the influence of FMO3 maturation) were compared, with the observed values in children aged 0-12 years.

Validation of the Developed PBPK Model Using Clinically Observed Data in Adults and Children

Human plasma concentration-time profiles after single oral administration of 500-mg ethionamide obtained from a published clinical study were used to test and verify the base model in adults.[10] In this study, ethionamide PK was determined in 12 healthy volunteers (3 Hispanic, 2 Indian, 7 white), aged 29-43 years, under fasted condition. In addition, a further clinical study conducted in 40 healthy subjects (aged 18-53 years) was used to validate the model (3 women and 37 men) after a single administration of 250-mg ethionamide[25] in formulations including sugar-coated and film-coated tablets. The sugar-coated tablet, which was the original ethionamide formulation, was reformulated in 2005 as a film-coated tablet.[25] Therefore, we assumed the clinical study that was conducted before 2005 used the sugar-coated tablet. Moreover, the film-coated tablet was shown to result in higher ethionamide bioavailability than the sugar-coated formulation after oral absorption (54% and 17% increase in C_{max} and AUC, respectively).[25] In this study, after comparison of the clinical study using sugar-coated tablets, the Caco-2 permeability of ethionamide was estimated by the application of the Simcyp parameter estimation module (using weighted least squares objective function and Nelder-Mead optimization methods)[36] to predict ethionamide permeability in the study using film-coated tablets. In vivo ethionamide PK data for the pediatric PBPK model validation were collected from the study conducted in children aged 3 months-13 years.[11] In association with the plasma concentration-time profiles, we collected dosing information, as well as demographic details such as age, sex, weight, and race.

Clinically observed PK data in the literature were used for the validation of all simulation models. The unreported individual data were extracted from figures within the original studies using GetData Graph Digitizer version 2.26. All simulations were constructed in accordance with the trial design used in the corresponding clinical studies, with particular parameters, including dose regimen, subject demographics, trial size, body weight, height, and ethnicities. The data entry process for the virtual clinical study design was performed in a manner similar to those in the respective observed trials. The detailed information used in all simulations of the present study is shown in Table 3.

Validation of the developed PBPK models was performed by visualization and comparison of the predicted/observed ratio of PK parameters and calculated success criteria. In data visualization, the observed plasma concentration-time data were overlaid with the simulated results. As reported by Abduljalil et al,[37] specific success criteria for PK parameter simulations should be calculated to consider the interindividual variability in the PK parameters of a drug in addition to the sample size of each clinical study. This principle was considered in determining the specific success criteria of the ethionamide PK parameters for each simulation in this study, as described below. The results are presented in Table 4.

Overall, the upper and lower limits can be written as $B\bar{x} \le X \le A\bar{x}$

$$A\bar{x} = \exp\left[\ln(\tilde{x}) + 4.26\frac{\sigma}{\sqrt{N}}\right] \quad (3)$$

and

$$B\bar{x} = \exp\left[\ln(\bar{x}) - 4.26\frac{\sigma}{\sqrt{N}}\right] \quad (4)$$

$$\sigma = \sqrt{\ln\left(\left(\frac{CV\%^2}{100}\right) + 1\right)}$$

$\bar{x}$: mean value of observed value
X: predicted value
$A\bar{x}$: limit of upper value
$B\bar{x}$: limit of lower value
N: sample size of clinical PK study
σ: standard deviation
CV: coefficient variability of observed data

Statistical Analysis

The results acquired from each experiment are shown as the mean ± standard deviation and were analyzed via Michaelis-Menten equation using GraphPad Prism 5 (San Diego, California) and SigmaPlot 8.0 (SPSS, Inc., Chicago, Illinois). The Pearson correlation analysis and linear regression were computed using R (version 3.4.3)[28] to analyze the association of predicted systemic clearance of FMO3 abundance with age. Analysis of covariance was performed with SPSS Statistics 23 (IBM, Armonk, New York) to compare predicted and observed systemic clearance while controlling for the effect of age. For all evaluations, $P < .05$ was considered significant. The individual in vivo ethionamide

Table 3. Details on the Parameters Used for Each Simulation in This Study

Study Design	Adult Model Simulations		Pediatric Model Simulation		
	250 mg single-dose in HVs[35]	500 mg single-dose in HVs[10]	0-2 years[11]	2-6 years[11]	6-12 years[11]
Population	General healthy north European white	Healthy north European white	Healthy pediatric white	Healthy pediatric white	Healthy pediatric white
Pop size	400 (10 trial[a]40)	120 (10 trials[a]12)	50 (10 trials[a]5)	60 (10 trials[a]6)	50 (10 trials[a]5)
Study duration	24 hours	24 hours	1 month	1 month	1 month
Dosing regimen	Single dose of 250 mg; fasted condition	Single dose of 500 mg; fasted	15-20 mg/kg once daily/fasted	15-20 mg/kg once daily/fasted	15-20 mg/kg once daily/fasted
Female proportion	0.075(3/40)	0.5 (6/12)	0.6 (3/5)	0.67 (4/6)	1 (5/5)
Age (years)	18-53	29-43	0-2	2-6	6-12
Weight (kg)[a]	74 ± 15.9	78 ± 9	8.3 ± 2.6	13.1 ± 2	26.1 ± 7.5
Height (cm)[a]	NA	174.3 ± 7	72.4	109.8	129.7
FMO3 abundance (pmol/mg protein)[b]	59.3 (38)	59.3 (38)	7.9 (75.4)	16.9 (58.2)	22.1 (49.6)
			$F = (\frac{Adult_{max} - F_{birth}}{Age_{50}^n + Age^n}) \times Age^n + F_{birth}$ (The values F_{birth}, $Adult_{max}$, Age_{50}, and n: 0.86, 25.95, 0.80 and 0.49, respectively)		
$CL_{int,FMO3}$ (μl/ min/mg microsomal protein)	13.43	13.43	6.43	13.43	13.43
CL_{lung} (L/h)	11.2	11.2	2.1	4.2	5.8

NA, not available; $Adult_{max}$, the maximum average relative protein abundance; Age, the age in years of the subject at the time of sample collection; Age_{50}, the age in years at which half-maximum adult protein abundance is obtained; F, the fractional protein abundance in adult samples; F_{birth}, the fractional protein abundance (of adult) at birth; HV, healthy volunteer; n, the exponential factor.

[a]Data presented as mean ± standard deviation.

[b]Data presented as mean (coefficient of variation).

clearance was generated from the clinical study using a Bayesian estimation with NONMEM software (version 7.4; GloboMax LLC, Ellicott City, Maryland).

Results

Ethionamide Metabolism in Pooled Human Liver and Lung Microsomes

K_m and V_{max} values of ethionamide sulfoxide formation from pooled human liver microsomes were 147.3 μM and 1987.9 pmol/min/mg protein, respectively. Similarly, the K_m and V_{max} values in pooled human lung microsomes were 52.3 μM and 4623.9 pmol/min/mg protein, respectively. The typical Michaelis-Menten graphs of the reaction velocity for the formation of ethionamide sulfoxide from ethionamide in human liver and lung microsomes are shown in Figure 2. Overall, the apparent CL_{int} value for ethionamide S-oxygenation in human liver microsomes was approximately one-sixth that in human lung microsomes.

Adult PBPK model development and validation.

Simulations of 500-mg and 250-mg single oral doses of ethionamide. A PBPK model of ethionamide was established through the incorporation of multiple levels of in vitro and clinical data and the consideration of the role of transporter-enzyme interplay in its disposition.[10,25] The developed PBPK model was utilized to simulate the PK profiles of single-dose ethionamide of 500-mg and 250-mg sugar-coated tablets. The predicted C_{max} (2.32 mg/L) and AUC (9.40 mg·h/L) were within 0.88- to 1.0-fold of the observed data (Table 4). The predicted ethionamide plasma concentration-time profiles adequately matched the clinical parameters for both 500-mg and 250-mg single oral administration of sugar-coated tablets within the prespecified acceptance criteria (Figure 3A and B). Subsequently, the Caco-2 permeability value was back-calculated at 87 (10^{-6} cm/s) to determine the time-concentration profile of ethionamide for the film-coated tablet. The simulated ethionamide exposure for the film-coated formulation was comparable with the observed data, within the predicted/observed ratio of 0.87-1.1 (Table 4 and Figure 3C). Overall, these results suggest that ethionamide PBPK models were reasonably developed based on in vitro and in vivo data.

The contribution of the enzyme and transporters to ethionamide disposition is shown in Figure 4. In particular, reducing the FMO3 activity to 0% resulted in a marked change in ethionamide C_{max} and clearance (56% and 44%, respectively; $P < .001$) compared with the control model. Collectively, the reduction of transporter activity by 100% in the intestine and liver caused a significant increase in C_{max} and clearance (103% and 20%, respectively) compared with the control model. Conversely, a minor effect in the alteration of ethionamide exposure with respect to clearance and C_{max}

Table 4. Comparison of PK Parameters for Simulations and Observed Data for Model Verification

	Simulated (n = 120)				Observed (n = 12)[10]			
500-mg Single Dose in Adults	C_{max} (mg/L)	T_{max} (h)	AUC (mg·h/L)	CL (L/h)	C_{max} (mg/L)	T_{max} (h)	AUC (mg·h/L)	CL (L/h)
Mean	2.32	1.6	9.4	56.74	2.3	1.7	10.0	64.5
CV%	29	42	25	26	59	51	36	24
Pred/Obs ratio	1.01	0.94	0.94	0.88				
Success criteria for Pred/Obs ratio	0.51-1.96	0.55-1.81	0.65-1.54	0.75-1.34				
	Simulated (n = 400)				Observed (n = 40)[35]			
250-mg Single Dose in Adults (Sugar-Coated Tablet)	C_{max} (mg/L)	T_{max} (h)	AUC (mg·h/L)	CL (L/h)	C_{max} (mg/L)	T_{max} (h)	AUC (mg·h/L)	CL (L/h)
Mean	1.66	1.31	5.37	49.90	1.48	1.5	6.5	NA
SD	0.48	0.34	1.42	13.52	0.6	0.9	1.78	NA
Pred/Obs ratio	1.12	0.87	0.83	NA				
Success criteria for Pred/Obs ratio	0.66-1.51	0.71-1.4	0.45-2.2	NA				
	Simulated (n = 400)				Observed (n = 40)[35]			
250-mg Single Dose in Adults (Film-Coated Tablet)	C_{max} (mg/L)	T_{max} (h)	AUC (mg·h/L)	CL (L/h)	C_{max} (mg/L)	T_{max} (h)	AUC (mg·h/L)	CL (L/h)
Mean	2.39	1.15	6.67	40.14	2.16	1.0	7.67	NA
SD	0.66	0.28	1.76	10.86	0.61	0.5	1.68	
Pred/Obs ratio	1.10	1.15	0.87	NA				
Success criteria for Pred/Obs ratio	0.66-1.51	0.71-1.4	0.45-2.2	NA				
	Simulated (n = 50)				Observed (n = 5)[11]			
0-2 Years (Sugar-Coated Tablet)	C_{max} (mg/L)	T_{max} (h)	AUC (mg·h/L)	CL (L/h)	C_{max} (mg/L)	T_{max} [a] (h)	AUC (mg·h/L)	CL (L/h)
Mean	3.11	1.20	8.58	21.82	3.79	0.97	7.84	22.01
SD	1.42	0.42	3.46	8.73	1.59	0.9-1.0	3.74	9.89
Pred/Obs ratio	0.82	1.23	1.09	1.00				
Success criteria for Pred/Obs ratio	0.74-1.34	0.68-1.46	0.56-1.77	0.50-2.02				
	Simulated (n = 60)				Observed (n = 6)[11]			
2-6 Years (Sugar-Coated Tablet)	C_{max} (mg/L)	T_{max} (h)	AUC (mg·h/L)	CL (L/h)	C_{max} (mg/L)	T_{max} [a, b] (h)	AUC (mg·h/L)	CL (L/h)
Mean	4.14	1.22	11.46	28.33	4.43	1.11	11.51	24.29
SD	1.55	0.42	3.77	10.02	1.23	0.9-2.1	6.9	8.93
Pred/Obs ratio	0.93	1.10	1.00	1.17				
Success criteria for Pred/Obs ratio	0.79-1.26	0.56-1.77	0.34-2.9	0.57-1.75				
	Simulated (n = 50)				Observed (n = 5)[11]			
6-12 Years (Sugar-Coated Tablet)	C_{max} (mg/L)	T_{max} (h)	AUC (mg·h/L)	CL (L/h)	C_{max} (mg/L)	T_{max} [a] (h)	AUC (mg·h/L)	CL (L/h)
Mean	4.41	1.40	13.12	39.52	3.62	2	13.54	34.49
SD	1.45	0.43	4.34	14.52	1.3	1.0-3.0	4.96	9.38
Pred/Obs ratio	1.22	0.70	0.97	1.15				
Success criteria for Pred/Obs ratio	0.78-1.28	0.68-1.46	0.57-1.75	0.47-2.11				

NA, not available; CV, coefficient of variation; SD, standard deviation; Pred/Obs ratio, predicted value/observed value ratio.

[a] Data presented as median (range).

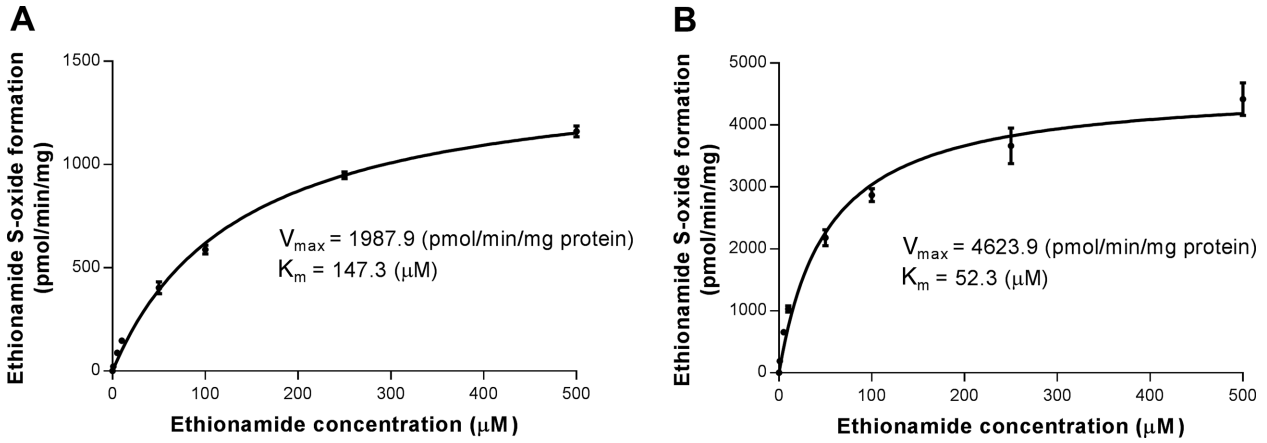

Figure 2. Formation kinetics of ethionamide sulfoxide. Michaelis-Menten curves show the formation kinetics of ethionamide sulfoxide over the ethionamide concentration range of 1 to 500 μM at pH 7.4 in pooled human liver (A) and pooled human lung (B) microsomes. Each point represents the average of triplicate incubations $\pm$ SD.

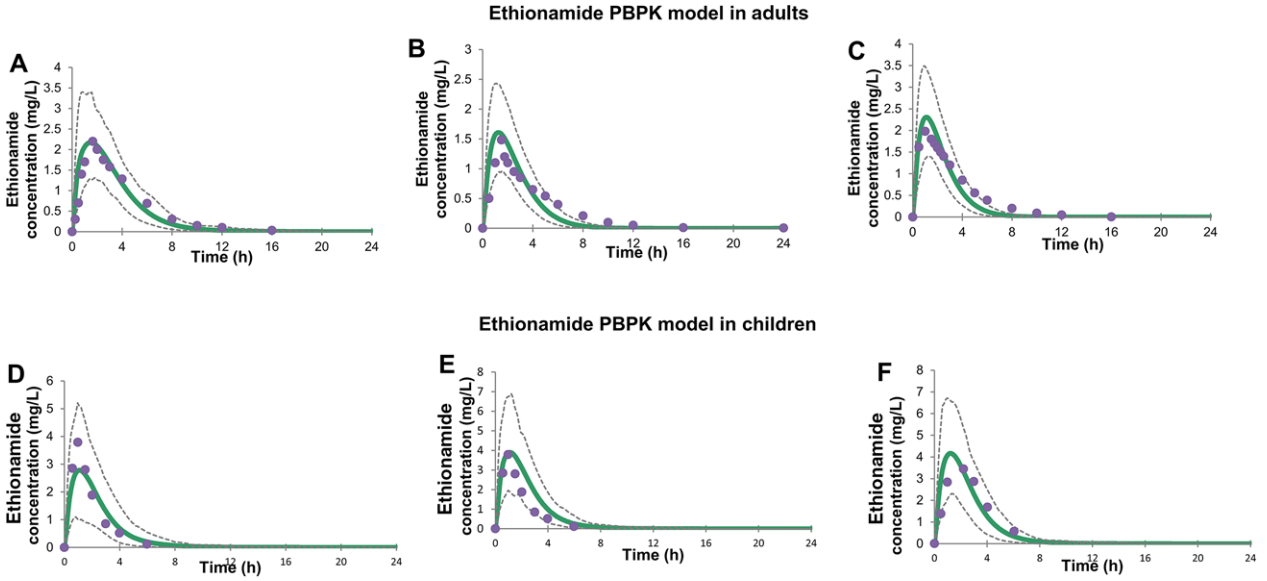

Figure 3. PBPK simulations of ethionamide pharmacokinetic profiles in adults and children. Time-concentration profiles of ethionamide in adults were described following a single oral dose of 500 mg sugar-coated tablet (A), 250 mg sugar-coated tablet (B), and 250 mg film-coated tablet (C). The concentration-time profiles of ethionamide in children were simulated across all age groups, including 0-2 years (D), 2-6 years (E), and 6-12 years (F). Green solid lines represent the mean of simulated ethionamide plasma concentrations with 95% confidence intervals, whereas filled circles represent the mean observed ethionamide plasma concentrations. Time-concentration profiles are shown in linear.

(only 10% and 8.9%, respectively) was observed, with a decrease in FMO2 functional catalysis ($P = .02$). Overall, ethionamide clearance was sensitive to reductions in FMO3 activity, whereas C_{max} was markedly increased by changes in transporter activity.

Ethionamide PBPK modeling in children. The Simcyp platform creates age-dependent anatomic and physiological characteristics for a virtual pediatric population based on the formula, illustrating the relationship between children's age and each value, as described previously.[24] The simulated plasma concentration-time profiles for 15 mg/kg once-daily administration of ethionamide in the pediatric population are shown in Figure 3D–F. Subsequently, validation of the developed pediatric PBPK models was performed using the observed data reported in clinical PK studies for children of the 3 age groups. Overall, the predicted/observed ratios of ethionamide PK parameters were all within the acceptance criteria, which suggests that ethionamide PBPK models appear reasonably well developed in the pediatric population for the in vitro absorption, distribution, metabolism, and excretion data, as well as FMO3 maturation.

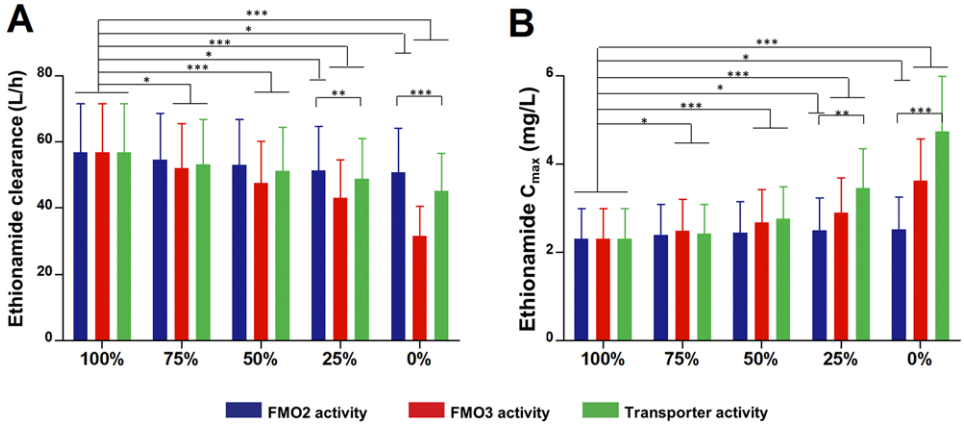

Figure 4. Effect of FMO2, FMO3, and transporter activity on predicted ethionamide clearance (A) and C_{max} (B) in virtual adults. Data are presented as mean + SD of the simulation results. *$P < .01$, **$P < .001$, ***$P < .0001$.

After simulation in 50-60 virtual pediatric patients for each age category (0-2, 2-6, and 6-12 years), the predicted clearances were 21.82, 28.33, and 39.52 L/h, respectively. The ratios of simulated to observed values were between 1.0 and 1.1 (Table 4). These simulations demonstrate that the current PBPK models were capable of accurate prediction of ethionamide exposure and elimination in children.

The well-predicted pediatric PBPK models were used to evaluate the effects of FMO3 maturation on ethionamide pharmacokinetics in children (Figure 5A) through the creation of a virtual duplicate with a 10-trial simulation. Consequently, by taking FMO3 maturation into account, a close match between the predicted and observed values and a significant correlation between clearance and age ($R^2 = 0.69$, $P < .001$) were observed. However, when FMO3 maturation was not taken into consideration, an overprediction of the PBPK-predicted total ethionamide clearance in the pediatric population and a weak correlation between clearance and age with $R^2 = 0.08$ ($P < .001$) were apparent compared with the observed data. One-way between-subject analysis of covariance was performed to examine the difference between observed value and simulated data (type of data), controlling for the effect of age. Because type of data had a significant effect on clearance after controlling for the effect of age ($F_{2,351} = 37.52$, $P < .001$) and age was a significant covariate ($F_{1,351} = 23.35$, $P < .001$), a post hoc test with Bonferroni correction was applied. Post hoc tests revealed a significant difference between observed and FMO3 maturation not considered data ($P < .001$), but no significant difference between observed and FMO3 maturation considered data ($P = 1.000$). Furthermore, a good association between FMO3 abundance and systemic clearance was observed, with $R^2 = 0.61$, $P < .001$, when the ontogeny of FMO3 in childhood was considered (Figure 5B), owing to the direct influence of age-related FMO3 protein expression, as well as its catalytic function.

Discussion

In the present study, we demonstrate that FMO3 maturation was associated with changes in ethionamide PK in children by considering the effect of transporter-enzyme interplay and FMO3 ontogeny over time on an ethionamide PBPK model.

In 2012, the FDA unanimously recommended modeling and simulation be considered for all pediatric drug development processes.[38,39] After the success of simulating PK in adult populations and the inherent ability of models to assist in the progress of extrapolation to different ages, the development of pediatric PBPK models could be considered a natural progression.[40] Extensive physiological changes occur during different periods of childhood, which significantly affect the pharmacokinetics/pharmacodynamics of drugs.[41] The ontogeny of drug-metabolizing enzymes will noticeably convert into age-related dosage changes for some drug therapies in pediatric patients. PBPK models incorporate multiple types of information, including in vitro, preclinical, and clinical profiles, thereby providing enhanced ability for the prediction and understanding of age-dependent PK alterations in the pediatric population.[38]

In addition to cytochromes P450 (CYPs), FMOs are critical for the oxidation of a wide range of therapeutic drugs, including nicotine, clozapine, sulindac sulfide, and ranitidine.[42] In contrast with CYPs, FMO3 expression has been reported to be stable, and interindividual variability due to environmental effects is highly improbable because FMO3 expression is widely unaffected by exogenous factors.[43] Although a number of PBPK models for CYP450-specific substrates[44,45] have been published, those for non-P450 enzymes,

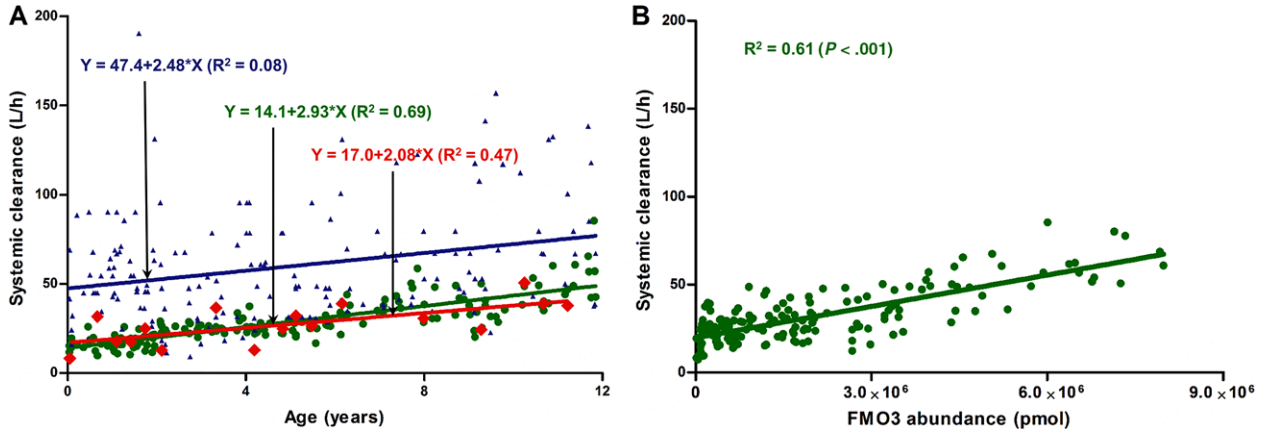

Figure 5. Scatterplots depicting the correlation of systemic clearance with age in children aged 0 to 12 years (A) and the relationship of FMO3 abundance with predicted systemic clearance (B). The correlation between predicted systemic clearance and age with consideration of FMO3 is expressed by the green regression line and without consideration of FMO3 maturation by the blue regression line. The green and blue symbols indicate the predicted individual systemic clearance with and without the presence of FMO3 ontogeny, respectively. The red line and square represent the regression line and the individual value of the clinically observed clearance reported in the literature, respectively.

including FMOs, are not well established, owing to limited knowledge of enzyme expression.[46] Nonetheless, FMO2 is selectively expressed in the lungs. The messenger RNA of FMO2 shows the greatest content among FMO forms in human lungs,[47] but isolation and purification of FMO2 protein from human lung tissues has been unsuccessful.[48] In addition, the principle of interindividual variability in FMO2 expression in humans depends on the presence of the enzymatically active protein (FMO2*1) or the truncated inactive protein (FMO2*2). The majority of global populations genotyped to date, including white and Asian populations, do not produce functionally active FMO2*1 in the lungs.[48] In this study, the expression and metabolic activity of FMO2 during childhood were considered to be similar to those observed in adults. This was supported by an animal study in which FMO2 expression was detected in the fetus and during the neonatal stage at levels similar to that observed in adult animals.[49] Notably, in this study, slight differences were found in the effect of FMO2 metabolic function on predicted ethionamide exposure (Figure 4). This can be explained adequately by the markedly lower scaling factor used to establish the lung model than the liver model. For the liver model, scaling factors were obtained from the Simcyp library, comprising an approximate mean value of 39.79 mg microsomal protein/g liver and 1744 g for liver weight, whereas the in vivo scaling factor for the lung was only 2.27 microsomal protein/g lung and 840 g for lung weight, as described in the method. Consequently, the estimation of in vivo clearance generated a greater value for the liver than for the lung, which can reasonably explain the minor contribution of FMO2 on ethionamide exposure (Figure 4). However, if the model is established in a black population, which possess the functionally active pulmonary form in a significant proportion of individuals (2%-27%),[9,42] the contribution of FMO2 to ethionamide PK could be larger. Accordingly, in this study, we focused on FMO3 maturation, specifically the functional metabolic capacity and ontogeny profile, which could explain the dynamic age-related changes in ethionamide PK in children.

Although ethionamide metabolism kinetic data have been reported previously[5] using recombinant human FMO2 and FMO3 enzymes, our data presented another approach to the determination of K_m and V_{max}, using pooled human liver and lung microsomes. In the present study, K_m of ethionamide in pooled human liver microsomes showed an acceptable match with a previous report using recombinant human FMO3.[5] However, the rate of metabolite formation by pooled human lung microsomes was lower than that by recombinant human FMO2 (83 μL/min/mg protein vs 12 μL/min/mg protein of enzyme). Differences in the in vitro metabolic system (ie, recombinant enzyme vs pooled human lung microsomes, pH = 9.5 vs pH = 7.4) may explain, at least in part, the differences between the studies.

Ethionamide is a class II drug (poor solubility and high permeability) in the Biopharmaceutical Drug Disposition Classification System,[50] and exhibits extensive metabolism and a predominant effect of efflux transporters in the gut and liver for oral dosing.[51] Consistent with this, our comprehensive in vitro transporter assay demonstrated that ethionamide was a potential substrate of P-gp, MRP1, and MRP2, but not of any solute carrier transporters (unpublished data). In this study, by taking advantage of PBPK simulation and modeling, we initially quantitated the contribution

of these efflux transporters on ethionamide disposition through the incorporation of ethionamide efflux kinetics by stably transfected LLC-PK1-MDR1, MDCKII-MRP1/MRP2 in the intestine and liver.

With regard to FMO3, its expression is low or negligible in the fetus and continuously increases to reach adult level in late childhood.[25] Collectively, the messenger RNA content of *FMO3* was found to be increased approximately 50-fold from fetal liver to adult liver.[47] Similarly, FMO3 abundance in neonatal liver was significantly lower compared with that observed in adults ($P < .001$).[15] The dynamic increase in the ontogenic expression of FMO3 could be a reasonable explanation not only for the substantial PK differences between children and adults, but also for differences in drug efficacy and toxicity during different stages of childhood.[52,53] In this study, through incorporation of FMO3 maturation, the predicted systemic clearance values showed good correlation with age across the 3 age ranges ($R^2 = 0.69$, $P < .001$) (Figure 5A) and were consistent with the results of a clinical PK study in children.[11] This observation indicates that integration of FMO3 maturation was essential to adequately describe the observed PK data in children in the PBPK model. Notably, this study indicates a strong linear relationship between FMO3 abundance and age-dependent increase in clearance (Figure 5B), or $R^2 = 0.61$. This finding demonstrates that the age-associated developmental changes in ethionamide PK were mainly supplied by FMO3 maturation. Consistent with our finding, Shimizu et al[16] indicated a significant correlation between trimethylamine *N*-oxygenation functional activity and FMO3 expression levels and developmental changes in functional metabolic capacity of FMO3 in childhood, using trimethylamine as a probe substrate.

Until recently, CYP- or carboxylesterase-specific probe substrate enzyme ontogenic profiles integrated in PBPK model were explored widely in a number of drugs, including tramadol,[54] acetaminophen,[55] oseltamivir,[29] and sotalol.[56] However, for FMO-substrate, only itopride's PBPK model was described to evaluate the impact of FMO3 polymorphism, by incorporating FMO3 activity and abundance.[57] Thus, our study is the first to apply FMO3 maturational changes from birth on the prediction of drug behavior.

The development and maturation of drug-metabolizing enzymes can affect various aspects of drug pharmacokinetics, especially in neonates and infants (eg, increase in peak-to-trough ratios or variability in exposure), which may modify a drug's efficacy and safety.[58] Clearly, the ontogenic profile of these enzymes will have to translate into age-dependent dosage adjustment in children for some drugs.[59] In our study, we indicate that the marked increase of FMO3 maturation from neonate to child is the most significant contributor to age-related changes of ethionamide pharmacokinetics. Currently, the application of our PBPK model to direct dosage recommendation is limited, mainly due to the lack of proper validation of our predictive performance.

There are some limitations to the present study. (1) The mean value of FMO3 abundance was not provided in the literature for age ranges similar to those in to the observed clinical study in children. Therefore, data extraction on individual subjects from the original study was performed to obtain the mean and coefficient of variation values for age groups that correspond to the observed data. (2) The clinical study in children was conducted in Africans, whereas our simulations were established in the white population, because data on African children were not available in the Simcyp population library. (3) The interindividual differences in FMO3 abundance or its catalytic activity may be derived partially from genetic polymorphisms of FMO3.[43] However, genotype was not considered in this study, and any genotype-related difference in FMO3 expression, catalytic activity, or ontogeny may have been disregarded in the simulations.

Conclusion

In conclusion, this is the first study to develop a PBPK model of ethionamide that considers comprehensive transporter-enzyme interplay and the effect of FMO3 maturation on ethionamide elimination in pediatric populations of different ages. The developed and validated model predicted ethionamide exposures accurately in both adult and pediatric populations using both opportunistic PK data and in-house data. This study indicated that the FMO3 maturational process in the pediatric population could primarily contribute to age-dependent developmental changes in ethionamide disposition. This approach could potentially be applied to determine the recommended dosing regimen of ethionamide in children to offer better patient outcomes and decrease toxicities.

Funding Information

This study was supported by a grant from the Korea Health Technology R&D Project through the Korea Health Industry Development Institute (KHIDI), funded by the Ministry of Health & Welfare, Republic of Korea (grant number HI15C1537).

Author Contributions

Participated in research design: Nguyen, Parvez, Kim, Ahn, Ghim, and Shin

Conducted experiments: Nguyen, Parvez, Kim

Analytic tools: Nguyen, Ghim, Shin

Performed data analysis: Nguyen, Kim, Lee, Ahn, Ghim, Shin

Wrote or contributed to the writing of the manuscript: Nguyen, Parvez, Lee, Ahn, Ghim, and Shin

Acknowledgments

We thank Sung-Eun Yoo for technical assistance. We declare no conflicts of interest or other relevant affiliations, financial involvement, or agreement/interest with any organization or governing body.

References

1. World Health Organization. Global tuberculosis report 2017.
2. World Health Organization. Treatment guidelines for drug-resistant tuberculosis, 2016 Update.
3. API TB Consensus Guidelines. API TB Consensus Guidelines 2006: management of pulmonary tuberculosis, extra-pulmonary tuberculosis and tuberculosis in special situations. *J Assoc Physicians India*. 2006;54:219–234.
4. Ettehad D, Schaaf HS, Seddon JA, Cooke GS, Ford N. Treatment outcomes for children with multidrug-resistant tuberculosis: a systematic review and meta-analysis. *Lancet Infect Dis*. 2012;12(6):449–456.
5. Henderson MC, Siddens LK, Morre JT, Krueger SK, Williams DE. Metabolism of the anti-tuberculosis drug ethionamide by mouse and human FMO1, FMO2 and FMO3 and mouse and human lung microsomes. *Toxicol Appl Pharmacol*. 2008;233(3):420–427.
6. Vannelli TA, Dykman A, Ortiz de Montellano PR. The antituberculosis drug ethionamide is activated by a flavoprotein monooxygenase. *J Biol Chem*. 2002;277(15):12824–12829.
7. Jenner PJ, Ellard GA, Gruer PJ, Aber VR. A comparison of the blood levels and urinary excretion of ethionamide and prothionamide in man. *J Antimicrob Chemother*. 1984;13(3):267–277.
8. Palmer AL, Leykam VL, Larkin A, et al. Metabolism and pharmacokinetics of the anti-tuberculosis drug ethionamide in a flavin-containing monooxygenase null mouse. *Pharmaceuticals (Basel)*. 2012;5(11):1147–1159.
9. Dolphin CT, Beckett DJ, Janmohamed A, et al. The flavin-containing monooxygenase 2 gene (*FMO2*) of humans, but not of other primates, encodes a truncated, nonfunctional protein. *J Biol Chem*. 1998;273(46):30599–30607.
10. Auclair B, Nix DE, Adam RD, James GT, Peloquin CA. Pharmacokinetics of ethionamide administered under fasting conditions or with orange juice, food, or antacids. *Antimicrob Agents Chemother*. 2001;45(3):810–814.
11. Thee S, Seifart HI, Rosenkranz B, et al. Pharmacokinetics of ethionamide in children. *Antimicrob Agents Chemother*. 2011;55(10):4594–4600.
12. Thee S, Garcia-Prats AJ, Donald PR, Hesseling AC, Schaaf HS. A review of the use of ethionamide and prothionamide in childhood tuberculosis. *Tuberculosis (Edinb)*. 2016;97:126-136.
13. Koukouritaki SB, Simpson P, Yeung CK, Rettie AE, Hines RN. Human hepatic flavin-containing monooxygenases 1 (*FMO1*) and 3 (*FMO3*) developmental expression. *Pediatr Res*. 2002;51(2):236–243.
14. Cherrington NJ, Cao Y, Cherrington JW, Rose RL, Hodgson E. Physiological factors affecting protein expression of flavin-containing monooxygenases 1, 3 and 5. *Xenobiotica*. 1998;28(7):673–682.
15. Xu M, Bhatt DK, Yeung CK, et al. Genetic and nongenetic factors associated with protein abundance of flavin-containing monooxygenase 3 in human liver. *J Pharmacol Exp Ther*. 2017;363(2):265–274.
16. Shimizu M, Denton T, Kozono M, Cashman JR, Leeder JS, Yamazaki H. Developmental variations in metabolic capacity of flavin-containing mono-oxygenase 3 in childhood. *Br J Clin Pharmacol*. 2011;71(4):585–591.
17. Pan Y, Hsu V, Grimstein M, et al. The application of physiologically based pharmacokinetic modeling to predict the role of drug transporters: scientific and regulatory perspectives. *J Clin Pharmacol*. 2016;56 (suppl 7):S122–S131.
18. Lave T, Dupin S, Schmitt C, Chou RC, Jaeck D, Coassolo P. Integration of in vitro data into allometric scaling to predict hepatic metabolic clearance in man: application to 10 extensively metabolized drugs. *J Pharm Sci*. 1997;86(5):584–590.
19. Lave T, Coassolo P, Ubeaud G, et al. Interspecies scaling of bosentan, a new endothelin receptor antagonist and integration of in vitro data into allometric scaling. *Pharm Res*. 1996;13(1):97–101.
20. Zou P, Yu Y, Zheng N, et al. Applications of human pharmacokinetic prediction in first-in-human dose estimation. *AAPS J*. 2012;14(2):262–281.
21. Parvez MM, Shin HJ, Jung JA, Shin JG. Evaluation of para-aminosalicylic acid as a substrate of multiple solute carrier uptake transporters and possible drug interactions with non-steroidal anti-inflammatory drugs in vitro. *Antimicrob Agents Chemother*. 2017;61(5).
22. Deshpande AY, Gurav S, Punde R, et al. Development and validation of a highly sensitive LC-MS/MS method for simultaneous quantitation of ethionamide and ethionamide sulfoxide in human plasma: application to a human pharmacokinetic study. *Biomed Chromatogr*. 2011;25(9):985–994.
23. Leong R, Vieira ML, Zhao P, et al. Regulatory experience with physiologically based pharmacokinetic modeling for pediatric drug trials. *Clin Pharmacol Ther*. 2012;91(5):926–931.
24. Johnson TN, Rostami-Hodjegan A, Tucker GT. Prediction of the clearance of eleven drugs and associated variability in neonates, infants and children. *Clin Pharmacokinet*. 2006;45(9):931–956.
25. Korth-Bradley JM, Mayer P, Mansfield D, Tucker H, Wu D. Comparative bioavailability study of single-dose film-coated and sugar-coated ethionamide tablets in healthy volunteers. *Clin Ther*. 2014;36(6):982–987.
26. Overby LH, Carver GC, Philpot RM. Quantitation and kinetic properties of hepatic microsomal and recombinant flavin-containing monooxygenases 3 and 5 from humans. *Chem Biol Interact*. 1997;106(1):29–45.
27. Haining RL, Hunter AP, Sadeque AJ, Philpot RM, Rettie AE. Baculovirus-mediated expression and purification of human FMO3: catalytic, immunochemical, and structural characterization. *Drug Metab Dispos*. 1997;25(7):790–797.
28. Team RC (2013) The R project for statistical computing. R Foundation for Statistical Computing. http://www.R-project.org/. Accessed April 4, 2018.
29. Boberg M, Vrana M, Mehrotra A, et al. Age-dependent absolute abundance of hepatic carboxylesterases (CES1 and CES2) by LC-MS/MS proteomics: application to PBPK modeling of oseltamivir in vivo pharmacokinetics in infants. *Drug Metab Dispos*. 2017;45(2):216–223.
30. Jamei M, Turner D, Yang J, et al. Population-based mechanistic prediction of oral drug absorption. *AAPS J*. 2009;11(2):225-237.

31. Rodgers T, Rowland M. Mechanistic approaches to volume of distribution predictions: understanding the processes. *Pharm Res*. 2007;24(5):918–933.
32. Prough RA, Sipal Z, Jakobsson SW. Metabolism of benzo(a)pyrene by human lung microsomal fractions. *Life Sci*. 1977;21(11):1629–1635.
33. Molina DK, DiMaio VJ. Normal organ weights in men: part II-the brain, lungs, liver, spleen, and kidneys. *Am J Forensic Med Pathol*. 2012;33(4):368–372.
34. Altman PL, Dittmer, DS, eds. *Growth—Including Reproduction and Morphological Development*. Washington, DC: Federation of American Societies for Experimental Biology; 1962.
35. McNally K, Cotton R, Loizou GD. A workflow for global sensitivity analysis of PBPK models. *Front Pharmacol*. 2011;2:31.
36. Jamei M, Marciniak S, Edwards D, et al. The Simcyp population based simulator: architecture, implementation, and quality assurance. *In Silico Pharmacol*. 2013;1:9.
37. Abduljalil K, Cain T, Humphries H, Rostami-Hodjegan A. Deciding on success criteria for predictability of pharmacokinetic parameters from in vitro studies: an analysis based on in vivo observations. *Drug Metab Dispos*. 2014;42(9):1478–1484.
38. Maharaj AR, Edginton AN. Physiologically based pharmacokinetic modeling and simulation in pediatric drug development. *CPT Pharmacometrics Syst Pharmacol*. 2014;3(11):1–13.
39. Huang SM, Rowland M. The role of physiologically based pharmacokinetic modeling in regulatory review. *Clin Pharmacol Ther*. 2012;91(3):542–549.
40. Poulin P, Jones RD, Jones HM, et al. PhRMA CPCDC initiative on predictive models of human pharmacokinetics, part 5: prediction of plasma concentration-time profiles in human by using the physiologically-based pharmacokinetic modeling approach. *J Pharm Sci*. 2011;100(10):4127–4157.
41. Marsousi N, Desmeules JA, Rudaz S, Daali Y. Usefulness of PBPK modeling in incorporation of clinical conditions in personalized medicine. *J Pharm Sci*. 2017;106(9):2380–2391.
42. Krueger SK, Williams DE. Mammalian flavin-containing monooxygenases: structure/function, genetic polymorphisms and role in drug metabolism. *Pharmacol Ther*. 2005;106(3):357–387.
43. Cashman JR, Zhang J. Human flavin-containing monooxygenases. *Annu Rev Pharmacol Toxicol*. 2006;46:65–100.
44. Varma MV, Lin J, Bi YA, et al. Quantitative prediction of repaglinide-rifampicin complex drug interactions using dynamic and static mechanistic models: delineating differential CYP3A4 induction and OATP1B1 inhibition potential of rifampicin. *Drug Metab Dispos*. 2013;41(5):966–974.
45. Hyland R, Dickins M, Collins C, Jones H, Jones B. Maraviroc: in vitro assessment of drug-drug interaction potential. *Br J Clin Pharmacol*. 2008;66(4):498–507.
46. Jones HM, Chen Y, Gibson C, et al. Physiologically based pharmacokinetic modeling in drug discovery and development: a pharmaceutical industry perspective. *Clin Pharmacol Ther*. 2015;97(3):247–262.
47. Zhang J, Cashman JR. Quantitative analysis of *FMO* gene mRNA levels in human tissues. *Drug Metab Dispos*. 2006;34(1):19–26.
48. Whetstine JR, Yueh MF, McCarver DG, et al. Ethnic differences in human flavin-containing monooxygenase 2 (*FMO2*) polymorphisms: detection of expressed protein in African-Americans. *Toxicol Appl Pharmacol*. 2000;168(3):216–224.
49. Larsen-Su S, Krueger SK, Yueh MF, et al. Flavin-containing monooxygenase isoform 2: developmental expression in fetal and neonatal rabbit lung. *J Biochem Mol Toxicol*. 1999;13(3-4):187–193.
50. Wu CY, Benet LZ. Predicting drug disposition via application of BCS: transport/absorption/elimination interplay and development of a biopharmaceutics drug disposition classification system. *Pharm Res*. 2005;22(1):11–23.
51. Shugarts S, Benet LZ. The role of transporters in the pharmacokinetics of orally administered drugs. *Pharm Res*. 2009;26(9):2039–2054.
52. Hines RN. The ontogeny of drug metabolism enzymes and implications for adverse drug events. *Pharmacol Ther*. 2008;118(2):250–267.
53. Hines RN. Developmental expression of drug metabolizing enzymes: impact on disposition in neonates and young children. *Int J Pharm*. 2013;452(1-2):3–7.
54. T'Jollyn H, Snoeys J, Vermeulen A, et al. Physiologically based pharmacokinetic predictions of tramadol exposure throughout pediatric life: an analysis of the different clearance contributors with emphasis on CYP2D6 maturation. *AAPS J*. 2015;17(6):1376–1387.
55. Jiang XL, Zhao P, Barrett JS, Lesko LJ, Schmidt S. Application of physiologically based pharmacokinetic modeling to predict acetaminophen metabolism and pharmacokinetics in children. *CPT Pharmacometrics Syst Pharmacol*. 2013;2:e80.
56. Khalil F, Laer S. Physiologically based pharmacokinetic models in the prediction of oral drug exposure over the entire pediatric age range-sotalol as a model drug. *AAPS J*. 2014;16(2):226-239.
57. Zhou W, Humphries H, Neuhoff S, et al. Development of a physiologically based pharmacokinetic model to predict the effects of flavin-containing monooxygenase 3 (FMO3) polymorphisms on itopride exposure. *Biopharm Drug Dispos*. 2017;38(6):389–393.
58. Rodieux F, Wilbaux M, van den Anker JN, Pfister M. Effect of kidney function on drug kinetics and dosing in neonates, infants, and children. *Clin Pharmacokinet*. 2015;54(12):1183-1204.
59. Lu H, Rosenbaum S. Developmental pharmacokinetics in pediatric populations. *J Pediatr Pharmacol Ther*. 2014;19(4):262-276.